Int. J. Disaster Risk Sci. 2011, 2 (4): 32–42
doi:10.1007/s13753-011-0018-3

ARTICLE

The MIKE Model Application to Overtopping Risk Assessment of Seawalls and Levees in Shanghai

Jun Wang*, Shiyuan Xu, Mingwu Ye, and Jing Huang

College of Resources and Environmental Science, East China Normal University, Shanghai 200062, China

Abstract This article used MIKE 21 models to evaluate the overtopping risk of seawalls and levees from the combined effect of land subsidence, storm tide, and sea level rise in Shanghai. Typhoon storm tides are the primary natural hazard affecting the Shanghai area. The worst storm tide in recent history was No. 9711, which produced a high tide of 5.99 m. Projections indicate that sea level will rise by 86.6 mm, 185.6 mm, and 433.1 mm by 2030, 2050, and 2100, respectively. The combined impact of these hazards threatens to flood large parts of the Shanghai area in the future. By 2030, 4.31 percent of the total length of the seawalls and levees in Shanghai will be at risk to being overtopped. By 2050, 27.55 percent of all seawalls and levees are likely to be overtopped. By 2100, overtopping will increase to 45.98 percent. The high risk of seawall and levee exposure to overtopping is closely related to the functional impact of land subsidence on the height of existing seawalls and levees. We propose specific engineering measures for Shanghai based on the results of our overtopping simulations.

Keywords MIKE model, multi-hazards, overtopping risk, Shanghai

1 Introduction

Coastal areas are frequently subject to the impact of natural hazards. Currently, 10 percent of the global population lives in low-lying coastal regions at elevations of just 0–10 m above sea level (McGranahan, Balk, and Anderson 2007). The Intergovernmental Panel on Climate Change report (IPCC 1995) shows that ongoing global climate change will cause the sea level to rise in coastal zones. Meanwhile, storm tides and subsidence will result in the permanent flooding of low-lying areas, inland extension of episodic flooding, increased beach erosion, and saline intrusion (Mclean and Tsyban 2001; Cooper, Beevers, and Oppenheimer 2008). Ongoing land subsidence amplifies sea level rise, which in turn amplifies storm tides, flooding, and erosion hazards. Sea level rise, storm tides, and land subsidence as multi-hazards will have a significant impact on environment, society, and economy (Stanley 1988; Dixon et al. 2006; Mazzotti et al. 2009).

Shanghai is low-lying, with an elevation of 3–4 m. The flood-control walls are currently more than 6 m high. Given the global trend of sea level rise and local issue of land subsidence, this is inadequate. The level of the East China Sea is rising at a rate of 3.0 mm a^{-1} (SOA 2010). Shanghai frequently suffers from extreme tropical storm tides. The risk of overtopping dikes is considerable. Since the 1990s, several studies have focused on the potential impact of sea level rise (Shi et al. 2000; Wu et al. 2003), storm tides (Duan, Qin, and Li 1998; Yu and Zhang 2002), land subsidence (Zuo, Liu, and Lin 1993; Gong, Li, and Yang 2009), and available measures for controlling them. Li, Qin, and Duan (1998) used historical tide records from seven tide gauge stations in the Shanghai area to analyze the mean annual eustatic sea level (MAESL) and fit it to a statistical model. These studies can help guide the implementation of disaster mitigation strategies in Shanghai. But due to data limitations, these studies lack comprehensive analysis of the combined effect of all three hazards.

In this research, we systematically collected data on sea level rise, storm tides, and land subsidence, and used MIKE 21 models to study the risk of seawalls and levees being overtopped from a combination of these three hazards. The study is divided into three sections: (1) we briefly consider the effects of sea level rise, storm tides, and land subsidence independently; (2) we present several scenarios and comprehensively assess overtopping risk for seawalls and levees under three disaster scenarios (2030, 2050, 2100); and (3) we present specific engineering suggestions for disaster mitigation measures in the Shanghai area.

2 Data and Methods

2.1 Geography

Shanghai is surrounded on three sides by the East China Sea, the Yangtze River Estuary, and Hangzhou Bay. The Yangtze River Estuary has a typical, sub-tropical monsoon climate

* Corresponding author. E-mail: jwang@geo.ecnu.edu.cn

with four distinct seasons. The average tidal amplitude of the estuary system ranges from 2.4 to 4.6 m, with an average of 2.6 m. The Yangtze River is the primary source of sediment for the wide continental shelf of the East China Sea. About 25 percent of the suspended sediment from the Yangtze is deposited in the coastal zone around the mouth of the river (Milliman et al. 1985). Coastal wetlands provide important land resources and serve as a buffer zone against natural disasters. The Yangtze River Estuary wetlands are mainly distributed in three regions. These include the Yangtze River Estuary islands (including the adjacent wetlands of the Chongming, Changxing, Hengsha, and Jiuduansha Islands), the middle Yangtze River Estuary wetlands, and the adjacent mainland wetlands (Wang et al. 2009) (Figure 1).

Coastal seawalls and flood-control levees have been built to combat the sea level rise and storm tides. Currently, Shanghai has 514 km of coastal seawalls. Only 23 percent of these seawalls can withstand a 200-year return period of storm tides and powerful category 12 typhoons (abbreviated as 200/12<, see Figure 2). Another 58 percent of the coastal seawalls will withstand a 100-year return period of storm tides and more than category 11 typhoons (abbreviated as 100/>11, Figure 2), while 19 percent of the coastal seawalls will only withstand a 100-year return period of storm tides but less than category 11 typhoons (abbreviated as 100/<11, Figure 2). Shanghai has 511 km of flood-control levees on the Huangpu River. About 58 percent of these levees can withstand a 1000-year return period of storm tides in the urban area (abbreviated as 1000, Figure 2), while the remaining levees can defend against a 50-year return period of tide in the Huangpu River (abbreviated as 50, Figure 2).

2.2 Data Sources and Hazards Analysis

2.2.1 Rise in Sea Level

We obtained data on the sea level rise for the Yangtze River Estuary and the East China Sea from three sources: (1) the Bulletin of Chinese Sea Level Rise (1978–2009) published by the State Oceanic Administration of China (SOA 2010); (2) historical annual mean tide gauge records (1912–1998) from the Wusongkou, Huangpu Park, and Luchaogang tide gauge stations (Li, Qin, and Duan 1998); and (3) published reports, particularly those by Qin and Li (1997).

We build upon Li, Qin, and Duan's (1998) work, which included data up to 1993, by including data through 2009.

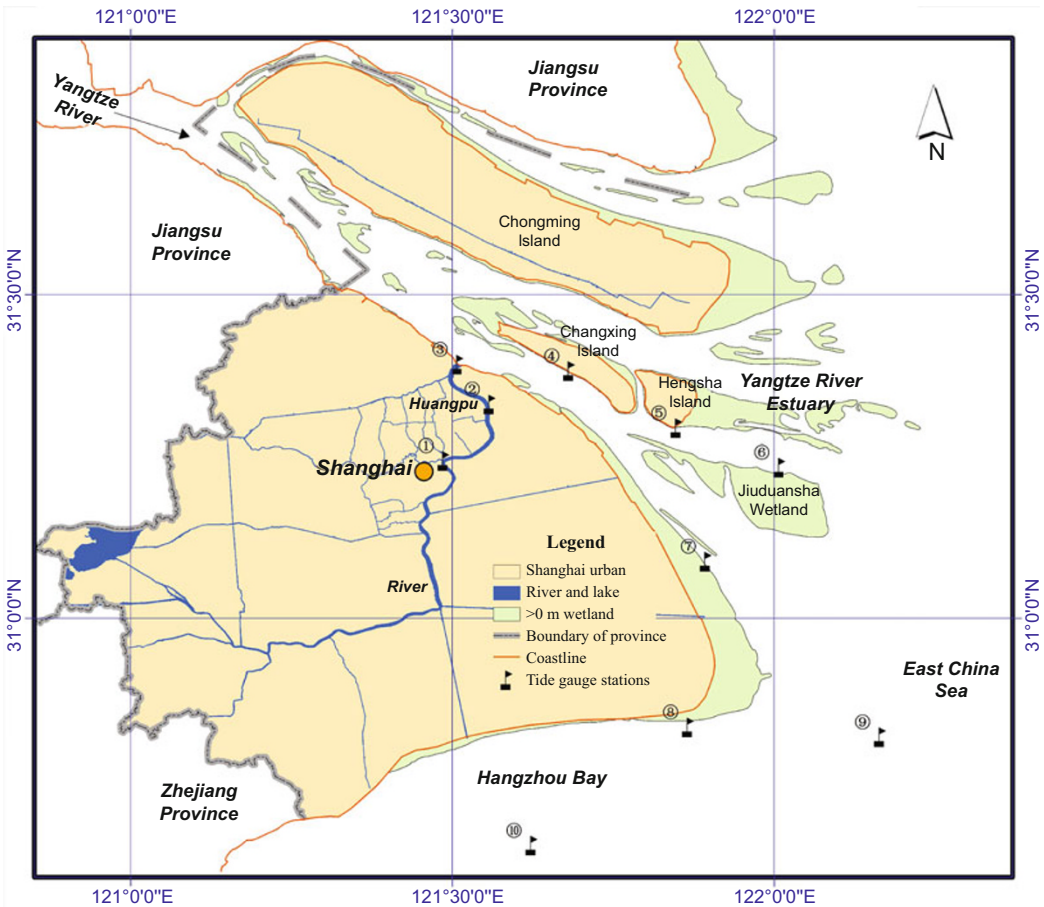

Figure 1. Map of the study area (Wetland distribution is based on the 2003 data)
Tide gauge stations: ① Huangpu Park, ② Waigaoqiao, ③ Wusongkou, ④ Changxing, ⑤ Hengsha, ⑥ Beicao, ⑦ Zhongjun, ⑧ Luchaogang, ⑨ Dajishan, ⑩ Tanhudao.

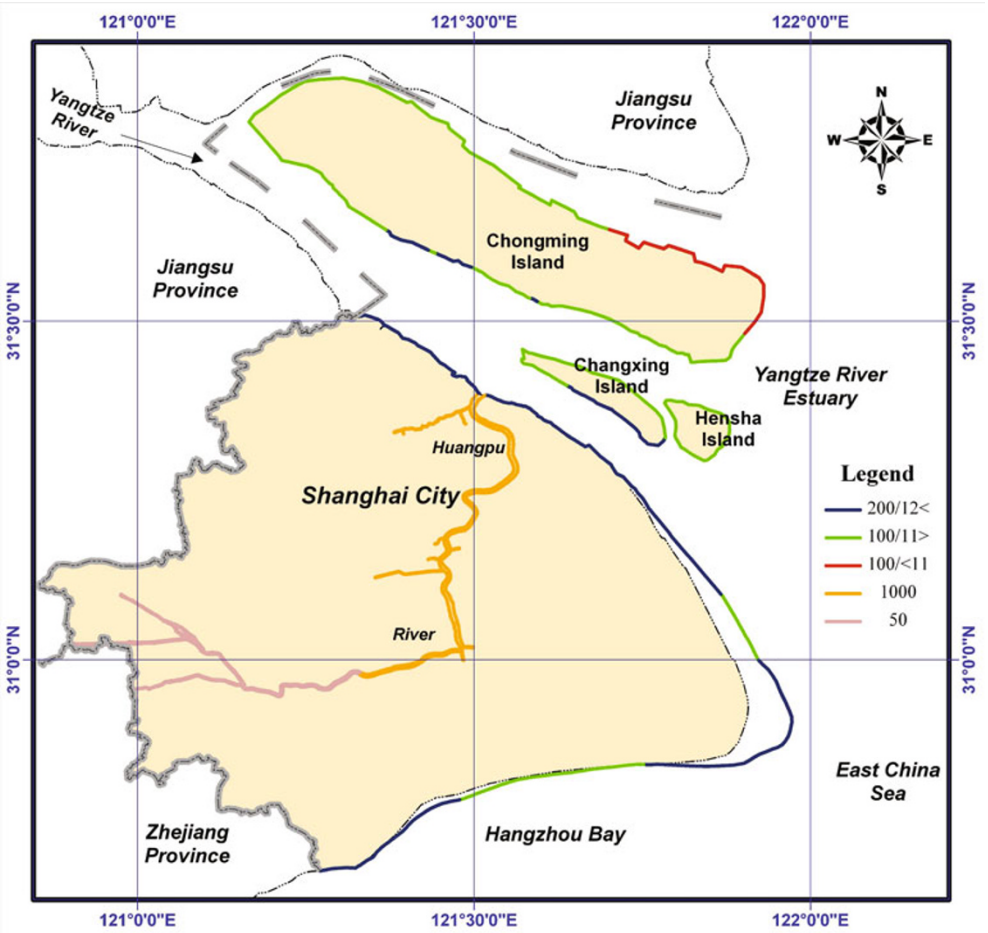

Figure 2. Coastal seawalls and flood-control walls in the Shanghai area

Li, Qin, and Duan adopted two measures to estimate the MAESL rise; we adopt their "second method." As shown in Table 1, Shanghai's eustatic sea level has increased over the past century and will continue to rise in the future. Projections indicate that the sea level will rise by 86.6 mm, 185.6 mm, and 433.1 mm by 2030, 2050, and 2100, respectively (Table 2).

2.2.2 Storm Tides

We collected tide level data for the most serious Shanghai storm tide (typhoon storm tide No. 9711, or Winnie) from ten tide gauge stations (Figure 2). At these tide stations, data were recorded every hour (from 00:00 on 18 August 1997 to 00:00 on 20 August 1997) throughout the course of storm tide 9711. Storm tide 9711 was caused by the combined effect of Typhoon Winnie and local high tides. The direct economic loss reached RMB 33.7 billion yuan, the greatest loss caused by storm tide event in China since 1949 (Le 2000). This storm tide formed in the Western Pacific on 10 August, and maintained a west-northwesterly path toward the East China Sea. According to the highest tide level at every tide gauge station, the tide level of storm tide 9711 reached a 300-year return period for the study area. The storm tide overtopped many of the coastal seawalls and dams and resulted in the flooding of much of the land these structures were intended to protect.

2.2.3 Land Subsidence

We obtained the spatial data on anthropogenic subsidence in the Shanghai area from the Shanghai Institute of Geological Survey's long-term monitoring of subsidence (1980–2005). From 1980 to 2005, the maximum accumulative subsidence was 6.04 m. According to an annual subsidence map, some portions of the coastlines of Chongming, Changxing, and Hengsha Islands rose slightly. The rest of the Shanghai area exhibited obvious subsidence with a maximum rate of 24.12 mm a^{-1}. Subsidence was greatest in five areas: central urban, northwestern, southwestern, and eastern areas of Shanghai, and the east coast of Chongming Island. Based on long-term monitoring with laser ranging and global positioning system technology, the Yangtze River Delta and adjacent areas are slow rate subsidence areas with an average neotectonic subsidence rate of 1.5 mm a^{-1} (Ye 1996).

Table 1. MAESL rise relative to 1990 for ten Shanghai tide gauge stations (unit: mm a^{-1})

Tide Station	Huangpu Park	Waigaoqiao	Wusong	Changxing	Hengsha	Zhongjun	Beicao	Luchaogang	Dajishan	Tanhudao
1997–2010	2	2.5	2.5	2.5	2.5	2.5	2.5	1.5	2.5	1
2011–2030	3	2.5	3	3	3	3	3	3.5	3	2
2031–2100	4.5	5	5	5	5	5	5	5	5	5

Note: MAESL data for Huangpu Park, Waigaoqiao, Wusong, and Luchaogang were from Li, Qin, and Duan (1998); MAESLs for Changxing, Hengsha, Zhongjun, Beicao, and Dajishan are based on the Wusongkou tide station data; and MAESL for Tanhudao is based on the Jinshan tide gauge station data.

Table 2. Eustatic sea level rise of Shanghai (unit: mm)

Scenarios	Huangpu Park	Waigaoqiao	Wusong	Changxing	Hengsha	Zhongjun	Beicao	Luchaogang	Dajishan	Tanhudao	Average Value
1997–2030	86	82.5	92.5	92.5	92.5	92.5	92.5	89.5	92.5	53	86.6
1997–2050	176	182.5	192.5	192.5	192.5	192.5	192.5	189.5	192.5	153	185.6
1997–2100	401	432.5	442.5	442.5	442.5	442.5	442.5	439.5	442.5	403	433.1

Note: 1997 is the base year for all scenarios.

2.2.4 Digital Elevation Model

We obtained high precision digital elevation points for the Shanghai urban area, the Yangtze River Estuary, and the Hangzhou Bay. Data from the urban area was provided by the Shanghai Municipal Bureau of Surveying and Mapping (year 2005). We extracted the Yangtze River Estuary data (year 2004) from the topographic map of the Shanghai coast (1:25,000), East China Sea charts (1:50,000), and the topographic map of the Hangzhou Bay (1:25,000). We obtained the map and elevation data for the coastal seawalls and Huangpu River levees from the Shanghai Water Authority (year 2009). We used ArcGIS 9.2 to build the DEM of the Shanghai area using the elevation points in the WGS84 coordinate system (Figure 3).

2.3 Combined Scenarios Design

Having examined the effects of the sea level rise, land subsidence, and storm tide separately, three scenarios were designed

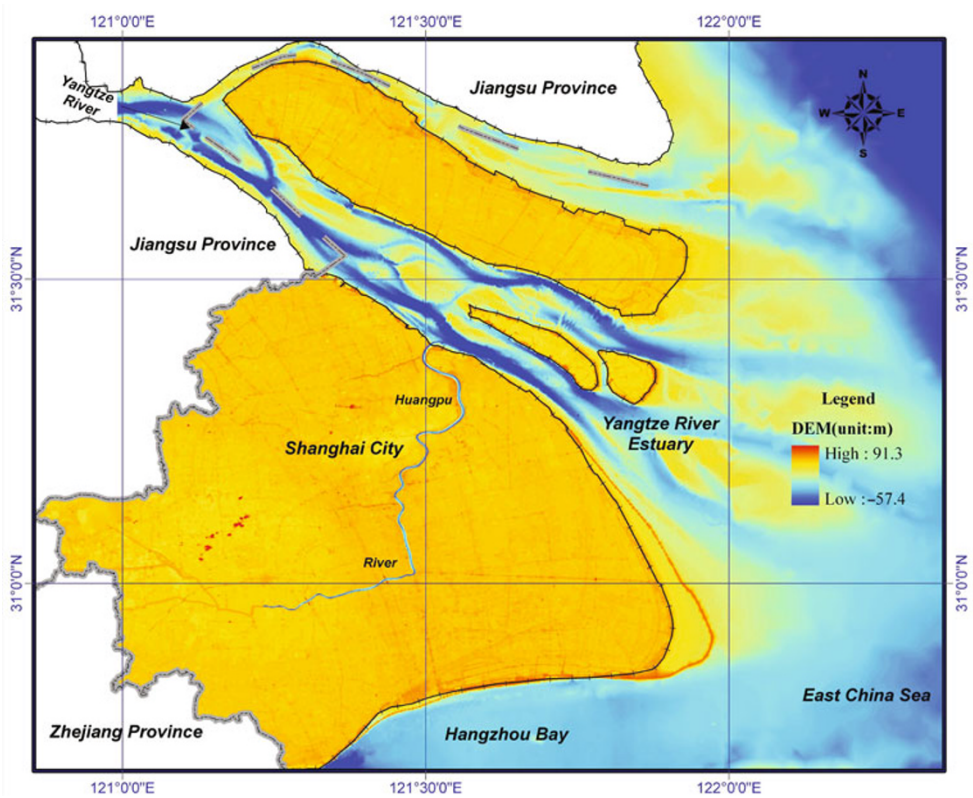

Figure 3. DEM of the study area

to investigate the combined effect of these three hazards. We make six assumptions: (1) the sea level rise at each tide gauge stations is that found in Table 1; (2) the neotectonic subsidence rate is at 1.5 mm a^{-1}; (3) the anthropogenic subsidence is the annual mean value from 1980 to 2005; (4) a typhoon storm tide comparable to 9711 occurs in each scenario; (5) seawalls, levees, and dams remain intact; and (6) limits in the drainage capacity of Shanghai's sewer systems will not be considered. Our three scenarios include predictions for 2030, 2050, and 2100 (Table 3).

2.4 Methods

2.4.1 Hydrodynamic and MIKE 21 Models

We used the MIKE 21 two-dimensional hydrodynamic model to simulate storm tides. The MIKE 21 hydrodynamic model is a general mathematical model for simulating variable, two-dimensional flow (DHI 2008). The MIKE 21 model uses the vertical average of two-dimensional shallow water equations, using discrete methods for calculating finite difference with the ADI (Alternating Direction Implicit) method and a double sweep algorithm. The equations for the model consist of the two momentum components (x and y) and an equation for the conservation of mass (Equations 1–3) (DHI 2008).

$$\frac{\partial \zeta}{\partial t}+\frac{\partial p}{\partial x}+\frac{\partial q}{\partial y}=\frac{\partial d}{\partial t} \quad \text{Eq. 1}$$

$$\frac{\partial p}{\partial t}+\frac{\partial}{\partial x}\left(\frac{p^2}{h}\right)+\frac{\partial}{\partial y}\left(\frac{pq}{h}\right)+gh\frac{\partial \zeta}{\partial x}+\frac{gp\sqrt{p^2+q^2}}{C^2\cdot h^2}-\frac{1}{\rho_w}\left[\frac{\partial}{\partial x}(h\tau_{xx})+\frac{\partial}{\partial y}(h\tau_{xy})\right] \quad \text{Eq. 2}$$
$$-\Omega_q-fVV_x+\frac{h}{\rho_w}\frac{\partial}{\partial x}(p_a)+F_x=0$$

$$\frac{\partial q}{\partial t}+\frac{\partial}{\partial y}\left(\frac{q^2}{h}\right)+\frac{\partial}{\partial x}\left(\frac{pq}{h}\right)+gh\frac{\partial \zeta}{\partial y}+\frac{gq\sqrt{p^2+q^2}}{C^2\cdot h^2}-\frac{1}{\rho_w}\left[\frac{\partial}{\partial y}\left(h\tau_{yy}\right)+\frac{\partial}{\partial x}\left(h\tau_{xy}\right)\right] \quad \text{Eq. 3}$$
$$+\Omega_p-fVV_y+\frac{h}{\rho_w}\frac{\partial}{\partial y}\left(p_a\right)+F_y=0$$

where x, y are the spatial coordinates; t is time; ζ is surface elevation; d is the time varying water depth; $h=\zeta-d$ is the total water depth; p, q are flux densities in x and y directions; C is the Chezy resistance, which is calculated from the Manning's number M following $C=M*h^{1/6}$; g is the acceleration due to gravity; f is the wind friction factor; V, V_x, and V_y are wind speed and the corresponding components in x and y directions, respectively; ρ_w is water density; τ_{xx}, τ_{xy}, and τ_{yy} are the components of bottom shear stress, respectively; F_x and F_y are the wave-induced momentum fluxes; p_a is the atmospheric pressure; and Ω_q, Ω_p are geostrophic effect.

2.4.2 Schema of Scenario Simulation

Based on the three scenarios presented in Table 3, we designed a schema of the technical route to simulate the overtopping risk from the combined effect of the hazards (Figure 4).

3 Storm Tide Model for the Yangtze River Estuary

3.1 Area and Elevation

The mathematical model includes predictions for Shanghai and its eastern coast. Using MIKE Flow Model, the maximum grid area is 0.6 km^2, the smallest grid angle is 26°, and the maximum number of grid nodes is 90,000.

3.2 Tidal Level Boundary

We used tide data from eight tide gauge stations from August 18, 00:00 to August 20, 00:00 (48 hours) to establish the tide time series (time interval of 1 hour) for the study area.

3.3 Wind Field

3.3.1 Specify Bathymetry

We considered the bathymetry of the study area in defining the grid on which the pressure and wind fields were computed. Typhoon winds occur in a rectangular grid. In order to cover the entire area, this rectangular grid must be larger

Table 3. The combined scenarios design for the Shanghai area

Year	Sea Level Rise[a]	Land Subsidence[b]	Storm Tides	Hazards Scenarios
2030	1997 used as the base year to predict the sea level rise in 2030	2005 used as the base year to predict the neotectonic and anthropogenic subsidence in 2030	Comparable to storm tide 9711	Based on the different scenarios, we model the potential combined risk of flooding in and around Shanghai
2050	1997 used as the base year to predict the sea level rise in 2050	2005 used as the base year to predict the neotectonic and anthropogenic subsidence in 2050		
2100	1997 used as the base year to predict the sea level rise in 2100	2005 used as the base year to predict the neotectonic and anthropogenic subsidence in 2100		

Note: [a] 1997 is used as the base year because this is when storm tide 9711 occurred; [b] 2005 is used as the base year because the DEM of the area was built using data from 2005.

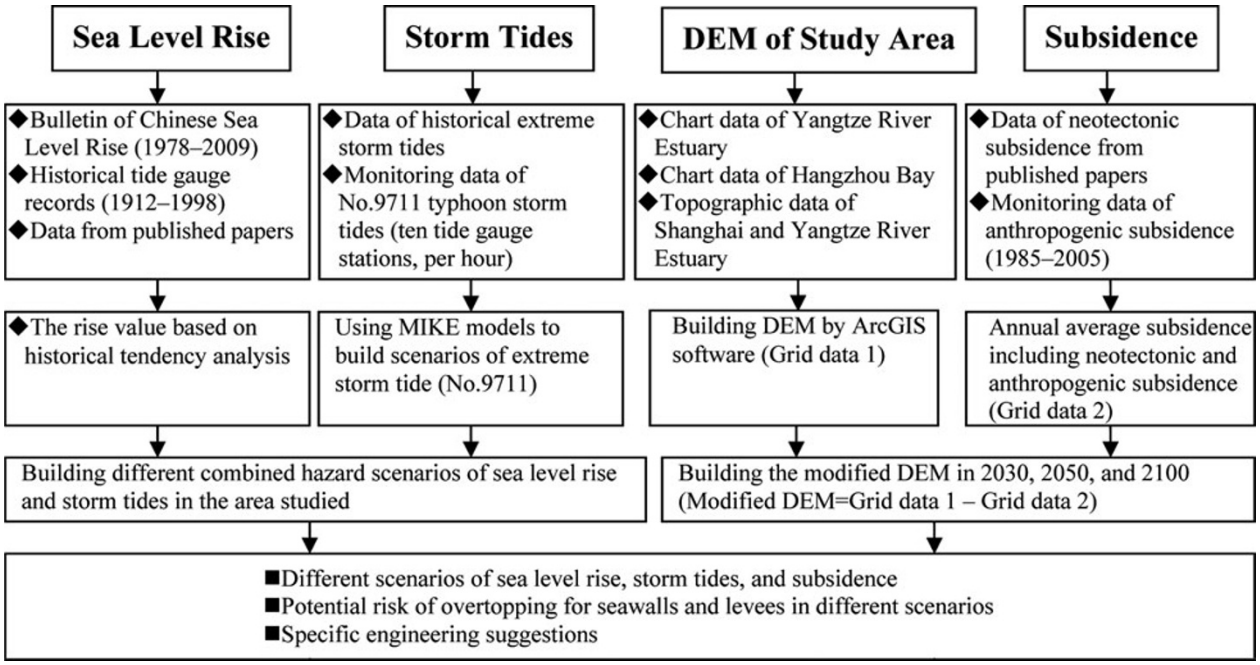

Figure 4. Flow chart for general methodology and analysis

than the mesh. The model region is 30°36′N–32°00′N and 120°48′E–122°24′E, with a 350 × 400 = 140,000 grid number, and an Ax = Ay = 400 m grid step.

3.3.2 Cyclone Lines

Cyclone lines contain the following eight parameters: (1) time in hours from the start of the cyclone period; (2) the longitude of the center of the cyclone (E positive and W negative, *x*-axis); (3) the latitude of the center of the cyclone (N positive, S negative, *y*-axis); (4) radius of maximum wind speed in km; (5) maximum wind speed in m s^{-1}; (6) central pressure in hPa; (7) neutral pressure in hPa (that is, the pressure outside the area affected by the cyclone); and (8) the rotational and translational components of the wind field. At a distance (R) from the center of the cyclone, the rotational wind speed (V_r) is:

$$V_r = V_{\max} \cdot (R/R_m)^7 \cdot \exp(7 \cdot (1 - R/R_m)) \quad \text{for} \quad R < R_m \qquad \text{Eq. 4}$$

$$V_r = V_{\max} \cdot \exp((0.0025 \cdot R_m + 0.05) \cdot (1 - R/R_m) \quad \text{for} \quad R \geq R_m \qquad \text{Eq. 5}$$

The translational component, V_t, is:

$$V_t = -0.5 \cdot V_f \cdot -(\cos\varphi) \qquad \text{Eq. 6}$$

The total wind speed, V, is:

$$V = V_r + V_t \qquad \text{Eq. 7}$$

Where, R_m is the radius of maximum wind speed; $V_{\max}$ is the maximum wind speed; V_f is the forward speed of cyclone center; and φ is the angle between due north and the maximum wind speed direction (DHI 2008).

The results include pressure, and the *x*- and *y*-components of wind, varying in time domain. The values for each grid point can be obtained using the vector operation for orthogonal synthesis. The dynamic changes of the wind model can be constructed and run in the MIKE HD water power module. The flow field of typhoon storm tide 9711 can be constructed in combination with the tidal boundary condition. We selected four tide gauge stations in the Yangtze River Estuary to validate the wind speed. Here, we use the Tanhudao and Dajishan tide gauge stations as examples. As shown in Figure 5, the predicted wind speed approximates the observed value, confirming the accuracy of the model.

3.3.3 Simulation Results and Verification

We used the tide data recorded at the Hengsha and Zhongjun tide gauge stations from 18 August 1997, 00:00 to 20 August 1997, 00:00 to verify the model. The most important factor affecting seawall security is the high tide level. Therefore, when the simulated high tide level is consistent with the measured high tide level, the model is considered accurate. The results show that in Hengsha and Zhongjun tide gauge stations the high tide simulation is accurate (Figure 6). Consequently, the model can be used for the Shanghai area.

4 Potential Threat to Seawalls and Levees

We used MIKE models to examine the three scenarios for storm surges and sea level rise. Based on the overtopping

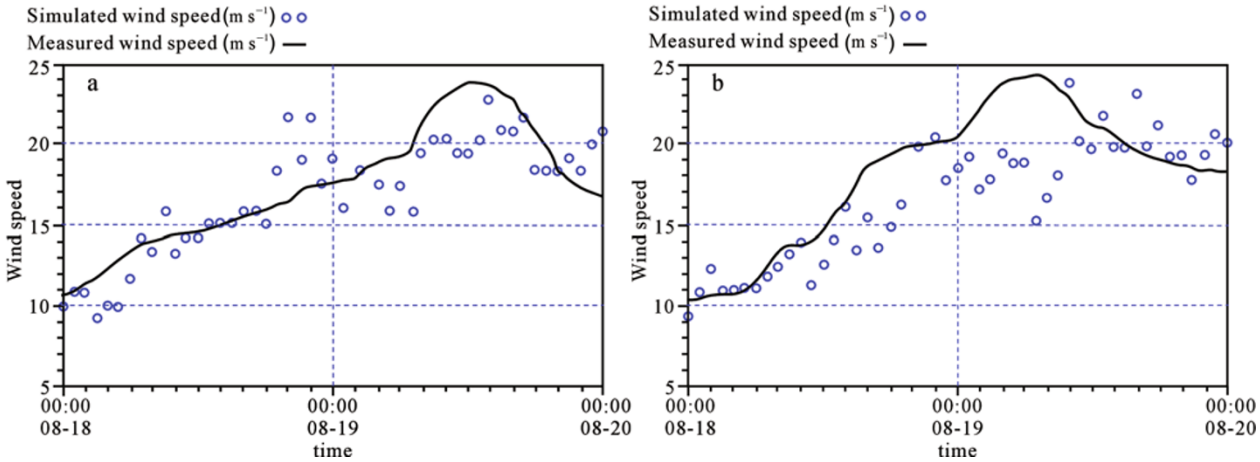

Figure 5. Comparison of measured and simulated wind speeds at (a) Tanhudao and (b) Dajishan tide gauge stations

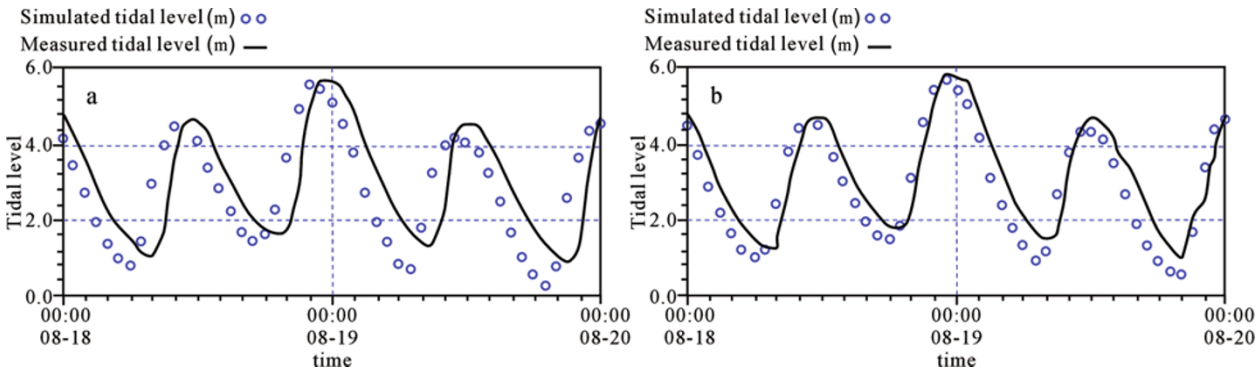

Figure 6. Comparison of measured and simulated tide levels at (a) Hengsha and (b) Zhongjun tide gauge stations

highest tide level in different sections of seawalls and levees, we divided the risk to seawalls and levees into five classes: first class, the overtopping tide level ≥ 0.4 m; second class, 0.3–0.4 m; third class, 0.2–0.3 m; forth class, 0.1–0.2 m; and fifth class, 0–0.1 m.

4.1 Potential Risk of Seawalls and Levees in 2030

The seawalls and levees on the south bank of Changxing Island, the west and south banks of Hengsha Island, and the adjacent bank of FX and NH will be threatened in 2030 (Figure 7). By 2030, overtopping will occur in 4.31 percent (35.42 km) of the total length of the seawalls and levees in Shanghai. In this scenario, the seawalls and levees largely will be able to protect the urban area (Table 4).

4.2 Potential Risk of Seawalls and Levees in 2050

The threat to seawalls and levees will be more serious in 2050 than that in 2030 (Figure 8). The length of seawalls at high risk will increase significantly and the Huangpu River levee will also be at high risk. The areas at greatest risk include the seawalls in JS and FX, and Changxing and Hengsha Islands, and the levees in SJ, PD, and BS. By 2050, overtopping will occur in 27.55 percent (226.77 km) of the total length of the seawalls and levees in Shanghai. The effectiveness of the seawalls and levees will decrease considerably, particularly the Huangpu River levees (Table 4).

4.3 Potential Risk of Seawalls and Levees in 2100

The threat to the seawalls and levees will increase considerably in 2100. The threat will be greatest on the south bank of Chongming Island, and the north banks of Changxing and Hengsha Islands (Figure 9). In addition, the length of the Huangpu River levees at high risk will increase significantly, particularly the levees closest to the central urban area. The total length of seawalls and levees at risk will be 378.43 km, or 45.98 percent of the total length of seawalls and levees. Thus, nearly half of the length of the seawalls and levees will be ineffective in protecting the urban area (Table 4).

5 Mitigation Strategies

Based on the 2005 DEM (without taking into account the effect of land subsidence between 2005 and 2100), the sea

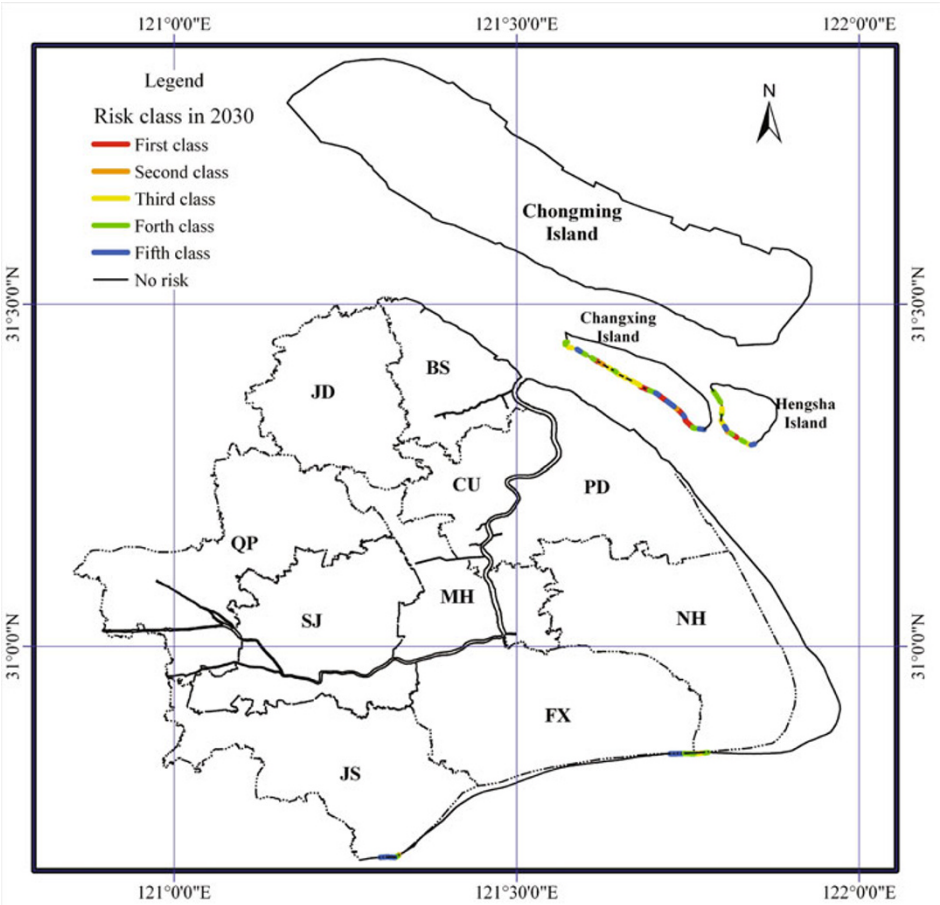

Figure 7. Risk of seawalls and levees in 2030

Abbreviations: Central Urban (CU) area, including Huangpu, Luwan, Xuhui, Changning, Jing'an, Putuo, Zhabei, Hongkou, and Yangpu Districts; Suburban area, including Pudong (PD), Nanhui (NH), Fengxian (FX), Jinshan (JS), Songjiang (SJ), Minhang (MH), Qingpu (QP), Jiading (JD), and Baoshan (BS) Districts, and Chongming County.

level rise predicted for 2100, and typhoon storm tide 9711, we also simulated the potential risk for overtopping of seawalls and levees in Shanghai in 2100. The overtopping risk is very low in this scenario. Thus, the main factor causing the overtopping projected in Section 4.3 is serious land subsidence, which decreases the height of seawalls and levees and reduces their effectiveness in protection against flooding.

We analyzed eight sections of the seawalls and levees to examine the impact of land subsidence: six sections of the Huangpu River levees (A–B: the upper south reach section, C–D: the upper north reach section, E–F: the Bund section, F–G: the Yangpu section, G–H: the Baoshan section, and I–J: the Pudong section) and two sections of the seawalls (K–L: the Jinshan section of Hangzhou Bay and M–N: the Changxing Island section on the south bank of the Yangtze River Estuary) (Figure 10). There are two reasons to choose these six sections: (1) the risk of overtopping is very high; (2) the potential economic damage is huge.

5.1 Flood-Control Levees along the Huangpu River

In the absence of land subsidence, the Huangpu River levees can withstand the extreme sea level rise and storm tide predicted for 2100. Based on the results of our analysis, we

Table 4. Risk of seawalls and levees in different scenarios

	Level of Risk	1	2	3	4	5	No Risk
2030	Length (km)	7.70	2.37	6.93	10.36	8.06	787.68
	Percentage (%)	0.94	0.29	0.84	1.26	0.98	95.69
2050	Length km)	(79.51	17.07	37.04	70.58	22.57	596.32
	Percentage %)	(9.66	2.07	4.50	8.58	2.74	72.45
2100	Length km)	(219.07	43.10	59.54	37.55	19.17	444.67
	Percentage %)	(26.62	5.24	7.23	4.56	2.33	54.02

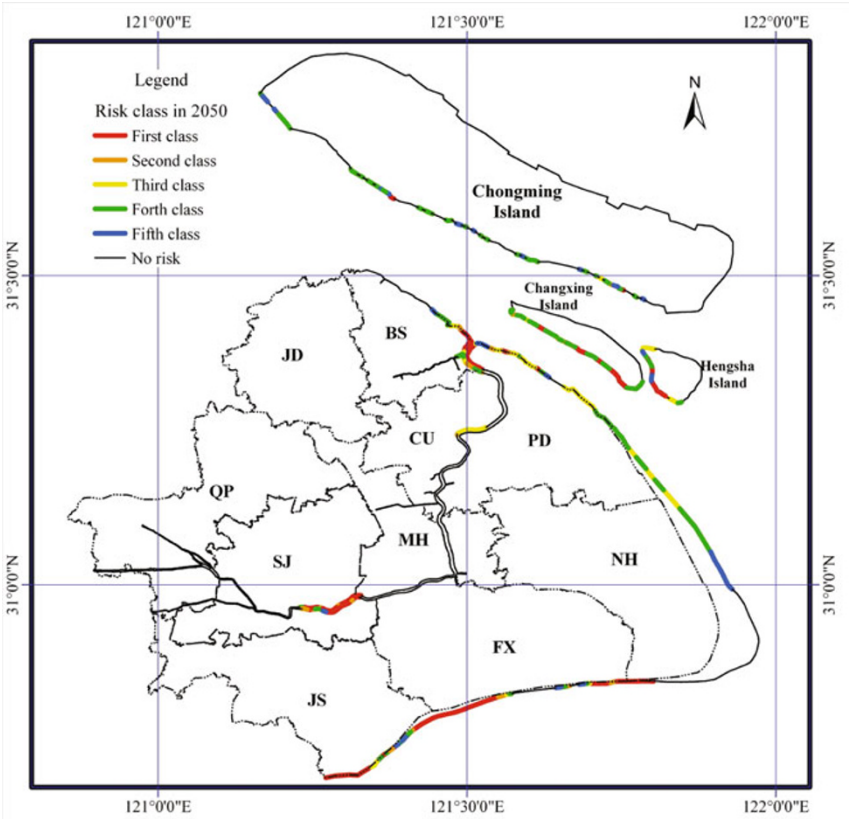

Figure 8. Risk of seawalls and levees in 2050

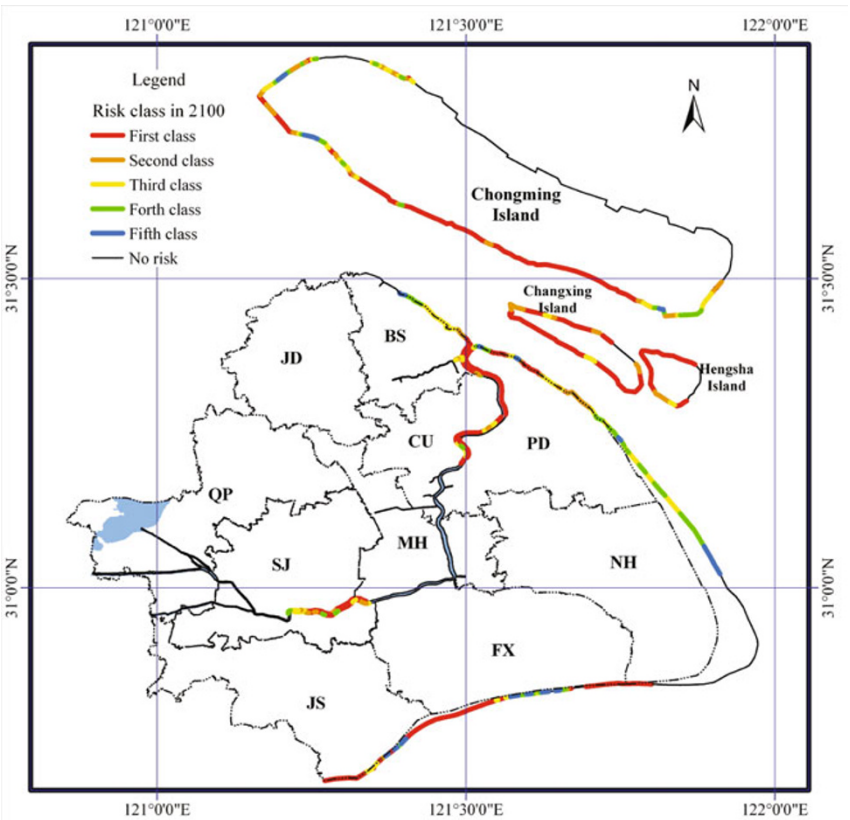

Figure 9. Risk of seawalls and levees in 2100

propose the concrete coping measures as follows: the upper reach of the Huangpu River levees should be raised by 0.66 m; the Bund reach of the Huangpu River levees needs to be raised by 1.44 m; the Yangpu section levee of the Huangpu River needs be heightened 1.37 m; the Baoshan section levee of the Huangpu River needs to be heightened 1.45 m; and the Pudong section levee of the Huangpu River needs to be heightened 1.32 m.

5.2 Flood-Control Seawalls in the Yangtze River Estuary

The Jinshan bank section is the portion of the seawalls most seriously affected by land subsidence. In order to improve the effectiveness of this seawall and the adjacent Nanhui, Fengxian, Pudong, and Baoshan seawalls, the height of these seawalls should be increased by 1.16 m. Although settlement on the three islands is minimal, the design standard of the seawalls on these islands was too low to be effective. The height of the Changxing and Hengsha Islands seawalls should be increased by 1.0 m, and that of Chongming Island should be increased by 0.8 m.

In addition, some scholars proposed that in order to lower the Huangpu River flood control pressure, Shanghai should build a flood barrier in Wusongkou. There are many famous flood-control structures throughout the world, including the Scheldt Delta storm tide barrier project in the Netherlands, the Thames tidal barrier in England, the St. Petersburg flood protection barrier in Russia, and the Venice flood barrier in Italy. Based on previous experience, the Shanghai water department and experts recommend the construction of the Wusongkou tide barrier. The best place to construct the barrier is the Changhang anchorage (Figure 10), 5.8 km from the mouth of the Huangpu River (Wusongkou). The barriers should be 8.5 m tall. The construction of the Wusongkou tide barrier will reduce the risk of flooding in Shanghai (Lu 2008). We think this proposal is worth considering.

6 Conclusions

The overtopping risk of seawalls and levees from the combined disaster effect of the three natural hazards is very high. In 2030, the total length of seawalls and levees affected will be 35.42 km. In 2050, the total length of seawalls and levees affected will be 226.77 km. In 2100, this number will be 378.43 km.

The potential impact of land subsidence on Shanghai's seawalls and levees is very serious and merits further attention. In the middle and lower reaches of the Huangpu River, and the seawalls near Shanghai's urban area, flood-control projects should take land subsidence into account. The height

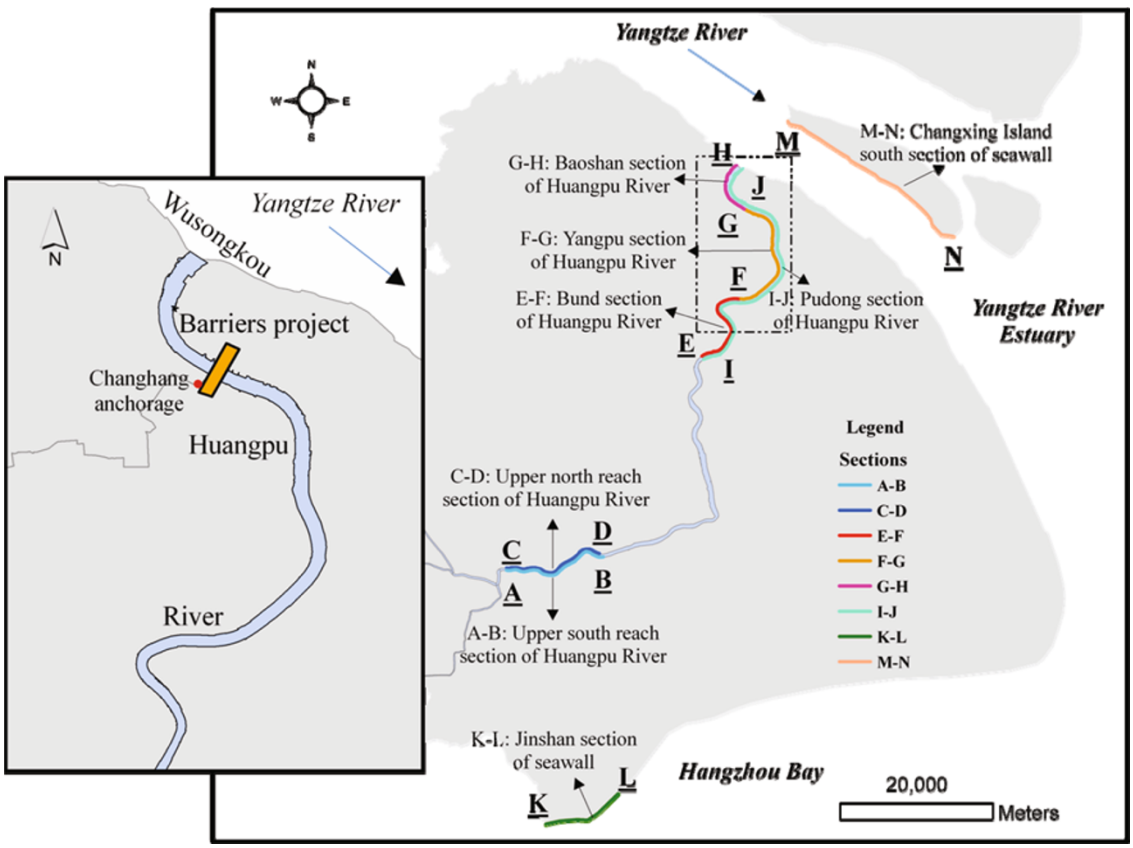

Figure 10. Seawall and levee sections examined in this study

of the Chongming, Changxing, and Hengsha Islands seawalls must be increased.

We used a MIKE model to build a two-dimensional hydrodynamic numerical model for the Yangtze River Estuary area. It was successfully used to simulate the effects of the multiple hazards of land subsidence, storm surges, and sea level rise. According to the comparison between the simulated results and the actual situation in the Shanghai area, we think that the techniques and methods in this study are reasonable. However, the validity of the results still needs to be further verified in our next step.

Acknowledgments

This article is jointly supported by the Fundamental Research Funds for the Central Universities and the Shanghai Youth Science and Technology Venus Program (Grants No. 09QA1401800). We wish also to extend our thanks to the anonymous reviewers who, despite their busy schedules, found the time to review this paper.

References

Cooper, M. J., M. D. Beevers, and M. Oppenheimer. 2008. The Potential Impacts of Sea Level Rise on the Coastal Region of New Jersey, USA. *Climatic Change* 90 (4): 475–92.

DHI (Danish Hydraulic Institute). 2008. *MIKE 21 Coastal Hydraulics and Oceanography, Hydrodynamic Module, Reference Manual*. Hørsholm, Denmark: DHI Water and Environment.

Dixon, T. H., F. Amelung, A. Ferretti, F. Novali, F. Rocca, R. Dokka, G. Sella, S. W. Kim, S. Wdowinski, and D. Whitman. 2006. Space Geodesy: Subsidence and Flooding in New Orleans. *Nature* 441 (7093): 587–88.

Duan, Y. H., Z. H. Qin, and Y. P. Li. 1998. Influence of Sea Level Rise on Shanghai Astronomical Tide and Storm Surge and Estimation of Probable Water Level. *Chinese Journal of Oceanology and Limnology* 16 (4): 298–307.

Gong, S. L., C. Li, and S. L. Yang. 2009. The Microscopic Characteristics of Shanghai Soft Clay and Its Effect on Soil Body Deformation and Land Subsidence. *Environmental Geology* 56 (6):1051–56.

IPCC (Intergovernmental Panel on Climate Change). 1995. *Climate Change 1994: Radiative Forcing of Climate Change and an Evaluation of the IPCC IS92 Emission Scenarios*. Cambridge: Cambridge University Press.

Le, K. T. 2000. An Analysis of the Recent Severe Storm Surge Disaster Events in China. *Natural Hazards* 21 (2–3): 215–23.

Li, Y. P., Z. H. Qin, and Y. H. Duan.1998. An Estimation and Assessment of Future Sea Level Rise in Shanghai Region. *Acta Geographica Sinica* 53 (5): 393–403 (in Chinese).

Lu Y. J. 2008. Shanghai's Storm Surge Defense Situation and Countermeasures. *Shanghai Water* 23 (4): 6–10 (in Chinese).

Mazzotti, S., A. Lambert, M. Van der Kooij, and A. Mainville. 2009. Impact of Anthropogenic Subsidence on Relative Sea-Level Rise in the Fraser River Delta. *Geology* 37 (9): 771–74.

McGranahan, G., D. Balk, and B. Anderson. 2007. The Rising Tide: Assessing the Risks of Climate Change and Human Settlements in Low Elevation Coastal Zones. *Environment and Urbanization* 19 (1): 17–37.

Mclean, R. F., and A. Tsyban. 2001. Coastal Zones and Marine Ecosystems. In *Climate Change 2001: Impacts, Adaptation, and Vulnerability*, edited by J. J. McCarthy. Cambridge: Cambridge University Press.

Milliman, J. D., H. T. Shen, Z. S. Yang, and H. M. Robert. 1985. Transport and Deposition of River Sediment in the Changjiang Estuary and Adjacent Continental Shelf. *Continental Shelf Research* 4 (1–2): 37–45.

Qin, Z. H., and Y. P. Li. 1997. Preliminary Study on the Sea Level Changes and Its Long-Term Prediction. *Acta Oceanologica Sinica* 19 (1): 1–9.

Shi, Y., J. Zhu, Z. Xie, Z. Ji, Z. Jiang, and G. Yang. 2000. Prediction and Prevention of the Impacts of Sea Level Rise on the Yangtze River Delta and Its Adjacent Areas. *Science in China (Series D)* 43 (4): 412–22.

Stanley, D. J. 1988. Subsidence in the Northeastern Nile Delta: Rapid Rates, Possible Causes, and Consequences. *Science* 240 (4851): 497–500.

SOA (State Oceanic Administration of the People's Republic of China). 2010. *Bulletin of Chinese Sea Level Rise*. http://www.soa.gov.cn/hyjww/hygb/A0207index_1.htm.

Wang, J., Z. Chen, D. Wang, X. Sun, and S. Xu. 2009. Evaluation of Dissolved Inorganic Nitrogen Eliminating Capability of the Sediment in the Tidal Wetland of the Yangtze Estuary. *Journal of Geographical Sciences* (2009) 19 (4): 447–60.

Wu, Q., X. Zheng, H. Xu, Y. Ying, Y. Hou, X. Xie, and S. Wang. 2003. Relative Sea-Level Rising and Its Control Strategy in Coastal Regions of China in the 21st Century. *Science in China (Series D)* 46 (1): 74–83.

Ye, S. H. 1996. *Movement Earth: The Research and Application of Crust Movement and Astro-Geodynamics*. Changsha: Hunan Scientific & Technical Publishing (in Chinese).

Yu, F. J., and Z. H. Zhang. 2002. Implementation and Application of a Nested Numerical Storm Surge Forecast Model in the East China Sea. *Acta Oceanologica Sinica* 21 (1): 19–31.

Zuo, H., T. Z. Liu, and X. H. Lin. 1993. Economic Benefit Risk Assessment of Controlling Land Subsidence in Shanghai. *Environmental Geology* 21 (4): 208–11.